

Topological edge states and disorder robustness in one-dimensional off-diagonal mosaic lattices

Ba Phi Nguyen

*Department of Basic Sciences, MienTrung University of Civil Engineering, Tuy Hoa 620000, Vietnam and
Mathematics and Physics Research Group, MienTrung University of Civil Engineering, Tuy Hoa 620000, Vietnam*

Kihong Kim*

*Department of Physics, Ajou University, Suwon 16499, South Korea and
School of Physics, Korea Institute for Advanced Study, Seoul 02455, South Korea*

(Dated: July 16, 2025)

We investigate topological edge states in one-dimensional off-diagonal mosaic lattices, where nearest-neighbor hopping amplitudes are modulated periodically with period $\kappa > 1$. Analytically, we demonstrate that discrete edge states emerge at energy levels $E = \epsilon + 2t \cos(\pi i/\kappa)$ ($i = 1, \dots, \kappa - 1$), extending the Su–Schrieffer–Heeger model to multi-band systems. Numerical simulations reveal that these edge states exhibit robust localization and characteristic nodal structures, with their properties strongly dependent on the edge configurations of long and short bonds. We further examine their stability under off-diagonal disorder, where the hopping amplitudes β fluctuate randomly at intervals of κ . Using the inverse participation ratio as a localization measure, we show that these topological edge states remain robust over a broad range of disorder strengths. In contrast, additional β -dependent edge states (emerging for $\kappa \geq 4$) are fragile and disappear under strong disorder. These findings highlight a rich interplay between topology, periodic modulation, and disorder, offering insights for engineering multi-gap topological phases and their realization in synthetic quantum and photonic systems.

I. INTRODUCTION

Topological insulators are quantum materials characterized by insulating bulk states and robust conducting edge or surface states [1, 2]. These unique properties have spurred significant interest in applications ranging from electronics and spintronics to quantum computing [3–5]. While early studies focused primarily on two-dimensional (2D) systems [6, 7], recent advances in experimental techniques and the conceptual simplicity of lower-dimensional models have shifted attention toward one-dimensional (1D) systems [8, 9].

To explore topological phenomena in 1D, various lattice models have been proposed [6, 10–12], incorporating both diagonal (on-site potential) and off-diagonal (hopping amplitude) modulations. Among these, the Su–Schrieffer–Heeger (SSH) model stands out as a paradigmatic example of 1D topological phases [10]. Originally developed to describe polyacetylene, the SSH model considers spinless fermions on a 1D lattice with staggered hopping amplitudes. Under periodic boundary conditions, it exhibits two distinct phases—trivial and nontrivial—distinguished by invariants such as the Zak phase [13]. In the nontrivial phase, open boundary conditions give rise to robust edge states, reflecting the bulk–boundary correspondence [4, 5].

Due to its simplicity and rich topological structure, the SSH model has been extensively studied and generalized [14–17]. Extended SSH models with three or more

sites per unit cell exhibit additional topological phases and edge states, depending on symmetry. For example, chiral edge states have been reported in inversion-symmetry-broken phases [14], and realizations of such models in optical and photonic systems have led to extensions into 2D structures with topological corner states [15]. Models with periodic hopping modulations of period four, analyzed using Chebyshev polynomials, have revealed multiple distinct edge phases supported by numerical simulations [16].

A more recent class of 1D lattice models—termed mosaic lattices—was introduced in [18], inspiring numerous studies on their physical properties [19–24]. In particular, the off-diagonal quasiperiodic mosaic lattice with modulated hopping amplitudes was shown to support topologically nontrivial phases with zero- and nonzero-energy edge states when the modulation is commensurate with the lattice [19]. For incommensurate modulations, Anderson localization arises from quasiperiodic off-diagonal disorder. In [20], introducing mosaic modulations in on-site potentials gave rise to a diagonal mosaic lattice model, where the interplay between modulation and superconducting pairing produced rich physical behavior. Furthermore, studies of disordered diagonal mosaic lattices revealed eigenstates at certain discrete energies exhibiting critical power-law localization, while all other states are exponentially localized [23, 24]. Experimental realizations of 1D topological phases have been demonstrated in diverse platforms, including ultracold atoms [25, 26], photonic crystals [27–29], electronic systems [30, 31], and non-Hermitian structures [32, 33].

In this work, we investigate the edge states of an off-diagonal mosaic lattice model, where nearest-

* khkim@ajou.ac.kr

neighbor hopping amplitudes are modulated periodically at equally spaced intervals with period κ . We also consider the effects of disorder, allowing the hopping amplitudes β to fluctuate randomly at intervals of κ . This model extends the off-diagonal quasiperiodic mosaic lattice of [19] by replacing quasiperiodic modulations with periodic or random ones, leading to several novel features. We show analytically that edge states emerge at discrete energy eigenvalues

$$E = \epsilon + 2t \cos\left(\frac{\pi}{\kappa}i\right), \quad i = 1, \dots, \kappa - 1, \quad (1)$$

where ϵ and t denote the on-site potential and (unmodulated) hopping amplitude, respectively. Numerical simulations reveal that these edge states exhibit robust localization and characteristic nodal structures, similar to those of critical states in disordered diagonal mosaic lattices [23, 24], with their properties strongly dependent on the edge configurations of long and short bonds. Using the inverse participation ratio (IPR) as a measure of localization, we demonstrate that these topological edge states remain robust over a broad range of disorder strengths. In contrast, additional β -dependent edge states, which emerge for $\kappa \geq 4$, are fragile and disappear under strong disorder.

II. THEORETICAL MODEL

We consider a standard tight-binding Hamiltonian for spinless electrons on a 1D lattice:

$$H = \sum_i \epsilon_i c_i^\dagger c_i + \sum_{\langle i,j \rangle} \left(t_{ij} c_i^\dagger c_j + t_{ij}^* c_j^\dagger c_i \right), \quad (2)$$

where c_i^\dagger and c_i are the creation and annihilation operators at site i , ϵ_i is the on-site potential, and t_{ij} ($= t_{ji}^*$) is the hopping amplitude from site j to site i . The sum $\langle i, j \rangle$ runs over distinct site pairs. Electron-electron interactions are neglected.

From Eq. (2), the discrete time-independent Schrödinger equation is

$$\epsilon_i \psi_i + \sum_j t_{ij} \psi_j = E \psi_i, \quad (3)$$

where ψ_i is the wave function amplitude at site i and E is the energy. Assuming nearest-neighbor hopping and uniform on-site potential $\epsilon_i = \epsilon$, Eq. (3) reduces to

$$\epsilon \psi_i + t_{i-1} \psi_{i-1} + t_i \psi_{i+1} = E \psi_i, \quad (4)$$

with $t_i \equiv t_{i,i+1} \in \mathbb{R}$ the hopping amplitude between sites i and $i+1$.

In the off-diagonal mosaic lattice model [20], hopping amplitudes are modulated as

$$t_i = \begin{cases} t\beta_i, & \text{if } i = j\kappa - m, \\ t, & \text{otherwise,} \end{cases} \quad (5)$$

where $\kappa > 1$ sets the mosaic modulation period, $j = 1, 2, \dots, J$, and $m \in [0, \kappa - 1]$ determines the edge configuration. The modulation factor β_i may be a constant (periodic case) or a random variable (disordered case). For purely off-diagonal systems, we set $\epsilon = 0$ in Eq. (4).

This study has two main objectives. First, we investigate the emergence of topological edge states in off-diagonal mosaic lattices, generalizing earlier results from extended SSH models [14–17]. We show analytically that for arbitrary κ , edge states appear at energies given by Eq. (1). Second, we examine the robustness of these edge states under disorder, a topic largely unexplored in the context of extended SSH-type models. Our results demonstrate that off-diagonal mosaic lattices support topological edge states that remain robust even under strong, spatially varying hopping modulations.

III. MULTI-BAND STRUCTURE AND EDGE STATES IN FINITE LATTICES

We analyze the periodic off-diagonal mosaic lattice with uniform modulation, $\beta_i = \beta$, focusing on the regime $\beta > 1$. For representative values of the inlay parameter $\kappa = 2, 3$, and 4, we demonstrate the emergence of edge states, with the results naturally extending to arbitrary integers $\kappa \geq 2$. We show that, for any such κ , edge states consistently emerge at all energy levels specified by Eq. (1).

A. Two-band model ($\kappa = 2$)

For $\kappa = 2$, the periodic off-diagonal mosaic model reduces to the well-known 1D SSH model, which describes spinless fermions on a 1D lattice with alternating strong and weak hopping amplitudes [10]. This model is a paradigmatic example of a 1D topological insulator, illustrating bulk–boundary correspondence and the emergence of topological edge states.

According to Eq. (5), when $m = 0$, the first bond has hopping amplitude t . For an even number of sites, $\beta > 1$ corresponds to weak coupling between the edge and the bulk, resulting in a nontrivial topological phase with edge states, while $0 < \beta < 1$ leads to strong edge coupling and a trivial phase [34]. A topological phase transition occurs at $\beta = 1$, where the band gap closes.

In the absence of on-site potential ($\epsilon = 0$), the Bloch Hamiltonian for $\kappa = 2$ under periodic boundary conditions is

$$H_{\kappa=2} = t \begin{pmatrix} 0 & \beta + e^{-2iq} \\ \beta + e^{2iq} & 0 \end{pmatrix}, \quad (6)$$

yielding the dispersion relation

$$\tilde{E}(q) = \pm \sqrt{1 + \beta^2 + 2\beta \cos(2q)}, \quad (7)$$

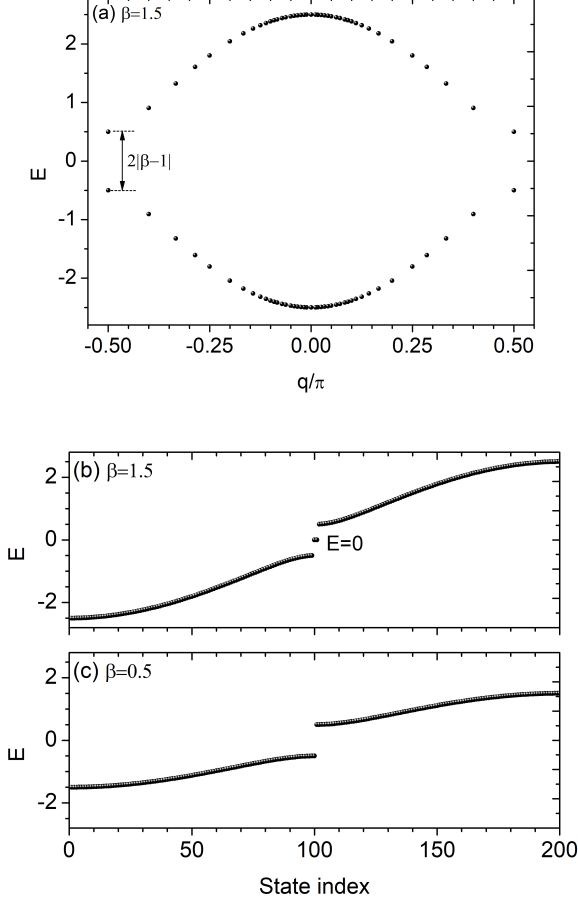


FIG. 1. (a) Energy E versus wavenumber q for $\beta = 1.5$ under periodic boundary conditions. A band gap opens at $q = \pm\pi/2$ when $\beta \neq 1$. (b, c) Energy E versus state index under open boundary conditions for $\beta = 1.5$ and $\beta = 0.5$, with $N = 200$ and $m = 0$. Two zero-energy edge states, localized at the left and right boundaries, appear for $\beta = 1.5$ but are absent for $\beta = 0.5$.

where $\tilde{E} = E/t$ and $q \in [-\pi/2, \pi/2]$. A band gap of width $\Delta\tilde{E} = 2|\beta - 1|$ opens at $q = \pm\pi/2$, separating two topologically distinct phases. For $\beta > 1$, zero-energy edge states appear under open boundary conditions, whereas no edge states exist for $0 < \beta < 1$ [12]. Hereafter, we set $t = 1$ and use \tilde{E} and E interchangeably when no confusion arises.

As shown in [16], when the number of sites N is even, a pair of degenerate zero-energy edge states emerges in the nontrivial phase ($\beta > 1$), while all states remain extended in the trivial phase. At the critical point $\beta = 1$, the hopping amplitudes are uniform, the gap closes, and the system becomes metallic.

Figure 1 shows the numerically computed energy spectrum for $N = 200$ and $m = 0$, with $\beta = 1.5$ and 0.5 . In the topologically nontrivial case, two zero-energy edge states are clearly visible. For odd N , only a single edge

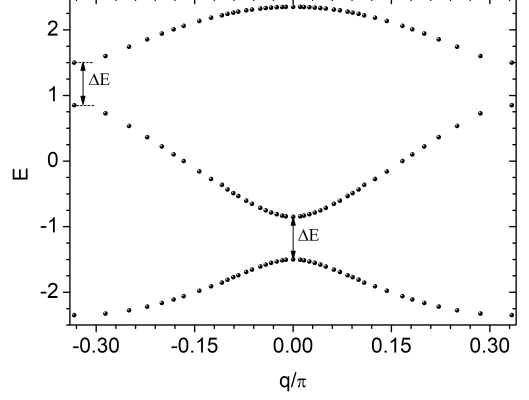


FIG. 2. Energy E versus wavenumber q ($-\pi/3 \leq q \leq \pi/3$) for $\beta = 1.5$ under periodic boundary conditions. For nonzero β , band gaps open at $q = 0$ and $q = \pm\pi/3$.

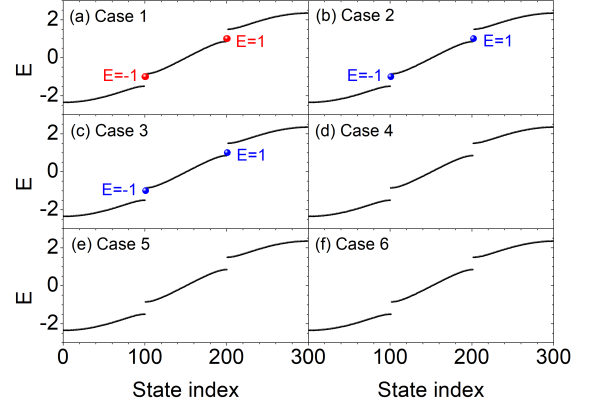


FIG. 3. Energy E versus state index for $\kappa = 3$ and $\beta = 1.5$ under open boundary conditions. The six configurations listed in Table I are shown separately. Red dots indicate doubly degenerate edge states localized at both boundaries, while blue dots denote single edge states localized at the left boundary.

state appears, localized at the left boundary.

B. Three-band model ($\kappa = 3$)

In this subsection, we analyze the case $\kappa = 3$. The spectrum of the model is determined by the eigenvalues of the Hamiltonian

$$H_{\kappa=3} = t \begin{pmatrix} 0 & \beta & e^{-3iq} \\ \beta & 0 & 1 \\ e^{3iq} & 1 & 0 \end{pmatrix}. \quad (8)$$

Diagonalizing this matrix yields the dispersion relation (with $t = 1$):

$$E^3 - (\beta^2 + 2)E - 2\beta \cos(3q) = 0, \quad (9)$$

TABLE I. Edge states for $\kappa = 3$ with $\beta > 1$. Here, m is defined in Eq. (5) and J is an integer. For each configuration, the numbers of long bonds at the left and right edges are specified.

Case no.	m	No. of sites	Left long bonds	Right long bonds	Left edge states	Right edge states
1	0	$3J$	2	2	$E = \pm 1$	$E = \pm 1$
2	0	$3J + 2$	2	1	$E = \pm 1$	None
3	0	$3J + 1$	2	0	$E = \pm 1$	None
4	1	$3J + 1$	1	1	None	None
5	1	$3J$	1	0	None	None
6	2	$3J + 2$	0	0	None	None

from which the band structure reduces to

$$E(q) = \sqrt{\frac{4a}{3}} \cos \left[\frac{\arccos(b)}{3} \right], \quad \sqrt{\frac{4a}{3}} \cos \left[\frac{\arccos(b)}{3} \mp \frac{2\pi}{3} \right], \quad (10)$$

where

$$a = \beta^2 + 2, \quad b = \left(\frac{3}{a} \right)^{3/2} \beta \cos(3q). \quad (11)$$

The band structure consists of three bands separated by gaps, forming asymmetric positive and negative branches. Band gaps open when $\beta \neq 1$. For example, for $\beta = 1.5$, numerical results (Fig. 2) show band gaps opening at $q = 0$ and $\pm\pi/3$, each with width $\Delta E \simeq 0.65$.

Edge states in finite lattices occur at $E = \pm 1$ (for $\epsilon = 0$), and their existence depends on the configurations of long (weak) bonds at the edges. Using the method in [16], we identify six independent edge configurations, summarized in Table I. Edge states appear only when at least one edge contains two long bonds. Numerical spectra for cases (a)–(f) (with $N = 300, 302, 301, 301, 300$, and 302 sites, respectively) are shown in Fig. 3. Red dots indicate pairs of degenerate edge states localized at both edges, while blue dots mark single edge states on the left edge. These results align perfectly with Table I.

The left-edge wave functions exhibit nodes at sites $i = 3j$ ($j = 1, 2, \dots$), located immediately to the left of short bonds ($t\beta$). The right-edge wave functions display mirror-symmetric nodes at all sites immediately to the right of short bonds. Representative wave functions for $E = 1$ in Case 1 are shown in Figs. 6(a) and 6(b).

C. Four-band model ($\kappa = 4$)

We next consider $\kappa = 4$. The Hamiltonian is given by

$$H_{\kappa=4} = t \begin{pmatrix} 0 & \beta & 0 & e^{-4iq} \\ \beta & 0 & 1 & 0 \\ 0 & 1 & 0 & 1 \\ e^{4iq} & 0 & 1 & 0 \end{pmatrix}. \quad (12)$$

Diagonalizing this yields (with $t = 1$):

$$E^4 - (\beta^2 + 3)E^2 + 1 + \beta^2 - 2\beta \cos(4q) = 0, \quad (13)$$

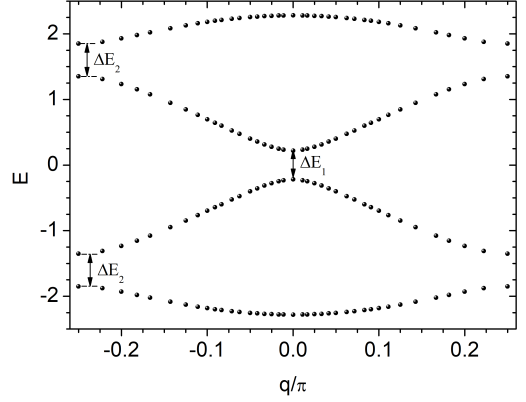


FIG. 4. Energy E versus wavenumber q ($-\pi/4 \leq q \leq \pi/4$) for $\beta = 1.5$ under periodic boundary conditions. For nonzero β , band gaps open at $q = 0$ and $q = \pm\pi/4$.

and the band structure

$$E(q) = \sqrt{\frac{A \pm \sqrt{B}}{2}}, \quad -\sqrt{\frac{A \pm \sqrt{B}}{2}}, \quad (14)$$

where

$$A = \beta^2 + 3, \quad B = \beta^4 + 2\beta^2 + 5 + 8\beta \cos(4q). \quad (15)$$

The spectrum has four symmetric bands separated by gaps. For $\beta = 1.5$, band gaps open at $q = 0$ and $q = \pm\pi/4$, with widths $\Delta E_1 \simeq 0.44$ and $\Delta E_2 \simeq 0.5$ (Fig. 4).

Edge states in a finite lattice appear at $E = 0, \pm\sqrt{2}$, and $\pm\sqrt{1 + \beta^2}$ (for $\epsilon = 0$). Their existence depends on the left and right edge configurations, which can be determined analytically using the results in [16]. There are ten independent configurations defined by the number of long (i.e., weak) bonds at each edge, as summarized in Table II. Edge states are present in all cases except for Case 5. Numerical energy spectra are shown in Fig. 5, where red dots indicate two degenerate edge states localized at opposite edges, and blue and violet dots denote nondegenerate edge states at the left and right edges, respectively. The total number of sites used for cases (a)–(j) are $N = 400, 403, 402, 401, 402, 401, 400, 400,$

TABLE II. Edge states for $\kappa = 4$ with $\beta > 1$. Here, m is defined in Eq. (5) and J is an integer. For each configuration, the numbers of long bonds at the left and right edges are specified.

Case no.	m	No. of sites	Left long bonds	Right long bonds	Left edge states	Right edge states
1	0	$4J$	3	3	$E = 0, \pm\sqrt{2}$	$E = 0, \pm\sqrt{2}$
2	0	$4J + 3$	3	2	$E = 0, \pm\sqrt{2}$	None
3	0	$4J + 2$	3	1	$E = 0, \pm\sqrt{2}$	$E = 0$
4	0	$4J + 1$	3	0	$E = 0, \pm\sqrt{2}$	$E = \pm\sqrt{1 + \beta^2}$
5	1	$4J + 2$	2	2	None	None
6	1	$4J + 1$	2	1	None	$E = 0$
7	1	$4J$	2	0	None	$E = \pm\sqrt{1 + \beta^2}$
8	2	$4J$	1	1	$E = 0$	$E = 0$
9	2	$4J + 3$	1	0	$E = 0$	$E = \pm\sqrt{1 + \beta^2}$
10	3	$4J + 2$	0	0	$E = \pm\sqrt{1 + \beta^2}$	$E = \pm\sqrt{1 + \beta^2}$

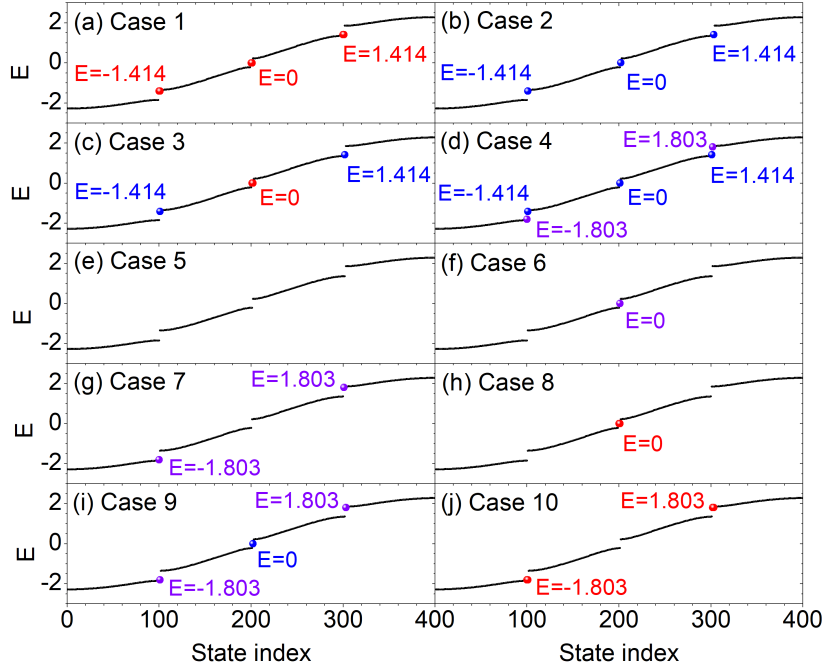


FIG. 5. Energy E versus state index for $\kappa = 4$ and $\beta = 1.5$ under open boundary conditions. The ten configurations listed in Table II are shown separately. Red dots indicate doubly degenerate edge states localized at both boundaries, while blue and violet dots represent single edge states localized at the left and right boundaries, respectively.

403, and 402, respectively. These numerical results are in perfect agreement with Table II.

Numerical results for the edge state wave functions in selected cases are shown in Figs. 6(c–h). For the eigenstates at $E = \pm\sqrt{2}$, the left-edge wave functions exhibit nodes at all sites immediately to the left of the short bonds with hopping amplitude $t\beta$, while the right-edge wave functions display mirror-symmetric nodes at all sites immediately to the right of the short bonds. For the $E = 0$ eigenstates, the left-edge wave functions have nodes both at all sites immediately to the left of the short bonds and at all sites midway between these positions. The right-edge wave functions again show mirror-symmetric nodes at the corresponding sites immediately

to the right of the short bonds and at the midway sites. The edge states at $E = \pm\sqrt{1 + \beta^2}$ exhibit distinct nodal patterns: the left-edge wave functions have nodes at all sites located one site further to the left from those immediately adjacent to the short bonds, while the right-edge wave functions have mirror-symmetric nodes at all sites one site further to the right from those immediately adjacent to the short bonds.

These results confirm that edge states occur at the energy eigenvalues specified by Eq. (1) for all $\kappa \geq 2$. Additional β -dependent edge states emerge for $\kappa \geq 4$, appearing only when at least one edge lacks long bonds, as summarized in Table II. The number and energy eigenvalues of these edge states are highly sensitive to the spe-

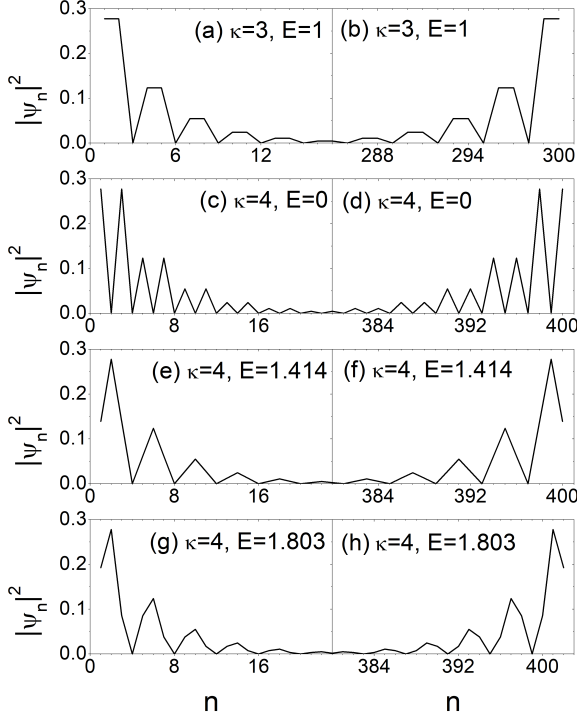


FIG. 6. Spatial distributions of eight selected edge-state wave functions for $\kappa = 3$ and 4 with $\beta = 1.5$. (a, b) States with $E = 1$ in Case 1 of Table I, with total site number $N = 300$. (c-f) States with $E = 0$ and $E = \sqrt{2}$ in Case 1 of Table II for $N = 400$. (g, h) States with $E = \sqrt{1 + \beta^2}$ in Case 10 of Table II for $N = 402$.

cific configurations of long and short bonds at the lattice edges.

D. Topological edge states for general κ

In this subsection, we prove that for any integer $\kappa > 1$, a finite off-diagonal mosaic lattice with open boundary conditions supports edge states at energy eigenvalues satisfying Eq. (1). Our approach closely follows the formalism developed in [16] for the $\kappa = 4$ case, which builds on the theorem established in [35].

The model described by Eq. (4) is a special case of a general three-term recurrence relation with periodic coefficients, $t_{i+\kappa} = t_i$. Following [16], we define $p_i = (t_1 t_2 \cdots t_i) \psi_{i+1}$. Starting from Eq. (4), it is straightforward to derive the relation

$$p_i = \varepsilon p_{i-1} - t_{i-1}^2 p_{i-2}, \quad (16)$$

where $\varepsilon \equiv E - \epsilon$. Imposing the boundary condition $\psi_0 =$

0, so that $p_{-1} = 0$, places Eq. (16) in the form analyzed in [35]. There it was shown that the solutions satisfy

$$p_{i\kappa+s} = h^{i-1} p_{\kappa+s} U_{i-1} \left(\frac{w}{2h} \right) - h^i p_s U_{i-2} \left(\frac{w}{2h} \right), \quad (17)$$

where U_i denotes the Chebyshev polynomials of the second kind, $w [= w(\varepsilon)]$ is a degree- κ polynomial obtained from

$$w(\varepsilon) = \frac{p_{2\kappa-1}(\varepsilon)}{p_{\kappa-1}(\varepsilon)}, \quad (18)$$

and, assuming all t_i are positive real numbers, h is defined as $h = t_1 t_2 \cdots t_\kappa$.

Substituting the definitions of p_i and h into Eq. (17) gives

$$\psi_{i\kappa+s} = \psi_{\kappa+s} U_{i-1}(\xi) - \psi_s U_{i-2}(\xi), \quad (19)$$

where $\xi \equiv w/(2h)$.

To prove the existence of edge states at energies $E = \epsilon + 2 \cos(\pi i/\kappa)$, we consider edge configurations where the first $(\kappa - 1)$ bonds on the left edge are long bonds, and the last $(\kappa - 2)$ bonds on the right edge are long bonds. This configuration corresponds to Case 2 in Tables I and II for $\kappa = 3$ and $\kappa = 4$, respectively. In such cases, edge states with energies $E = \epsilon + 2 \cos(\pi i/\kappa)$ appear only on the left edge, and no β -dependent edge states are present. The total number of lattice sites is $N = \kappa J + \kappa - 1$ for an arbitrary large integer J .

For edge states to exist on the left boundary, the wave function at site $N + 1 = \kappa(J + 1)$ must vanish. From Eq. (19), this condition reads

$$\begin{aligned} \psi_{\kappa(J+1)} &= \psi_{2\kappa} U_{J-1}(\xi) - \psi_\kappa U_{J-2}(\xi) \\ &= \psi_\kappa \left[\frac{\psi_{2\kappa}}{\psi_\kappa} U_{J-1}(\xi) - U_{J-2}(\xi) \right] = 0. \end{aligned} \quad (20)$$

In the periodic off-diagonal mosaic lattice, $t_1 = t_2 = \cdots = t_{\kappa-1} = t (= 1)$ and $t_\kappa = t\beta (= \beta)$. Using the periodicity of t_i and Eq. (18), we find

$$\frac{\psi_{2\kappa}}{\psi_\kappa} = \frac{w}{t_1 t_2 \cdots t_\kappa} = 2\xi. \quad (21)$$

Substituting this relation and employing the recursion $U_J(\xi) = 2\xi U_{J-1}(\xi) - U_{J-2}(\xi)$ in Eq. (20) yields $\psi_\kappa = 0$, provided $U_J(\xi)$ does not identically vanish. This result implies that the wave function exhibits nodes at all sites $i = \kappa j$ for $j = 1, 2, \dots$.

From Eq. (4), we obtain

$$\begin{aligned} -\varepsilon \psi_1 + \psi_2 &= 0, \\ \psi_1 - \varepsilon \psi_2 + \psi_3 &= 0, \\ &\vdots \\ \psi_{\kappa-2} - \varepsilon \psi_{\kappa-1} + \psi_\kappa &= 0. \end{aligned} \quad (22)$$

These $(\kappa - 1)$ equations can be written compactly as

$$\psi_{i-1} - \varepsilon \psi_i + \psi_{i+1} = 0, \quad (23)$$

for $i = 1, 2, \dots, \kappa - 1$. Comparing this with the recurrence relation of Chebyshev polynomials $U_i(\varepsilon/2)$, we identify $\psi_i = U_{i-1}(\varepsilon/2)$, implying $\psi_\kappa = U_{\kappa-1}(\varepsilon/2)$. Since the zeros of $U_n(x)$ are at $x = x_k$ when $x_k = \cos[k\pi/(n+1)]$ for $k = 1, 2, \dots, n$, ψ_κ vanishes when

$$\frac{\varepsilon}{2} = \cos(k\pi/\kappa), \quad k = 1, 2, \dots, \kappa - 1. \quad (24)$$

Therefore edge states exist when the energy satisfies $E = \epsilon + 2\cos(\pi i/\kappa)$ with $i = 1, 2, \dots, \kappa - 1$.

IV. ROBUSTNESS OF EDGE STATES UNDER DISORDER

In the periodic off-diagonal mosaic model, our analysis shows that nearly all states correspond to extended bulk states, except for specific in-gap edge states that are exponentially localized at the boundaries of a finite chain. While numerous studies have demonstrated that zero-energy edge states are topologically protected against disorder [12], the stability of nonzero-energy edge states under disorder remains less well explored. To address this, we investigate their behavior within a disordered off-diagonal mosaic lattice chain, where β_i in Eq. (5) are independent random variables uniformly distributed in the interval $[\beta_0 - W/2, \beta_0 + W/2]$, with β_0 denoting the average value of β_i . The parameter W characterizes the disorder strength, while all other hopping amplitudes are fixed at $t = 1$.

Before presenting the numerical analysis, we briefly discuss the $\kappa = 1$ case without mosaic modulation. In this limit, it is well known that purely off-diagonal disorder leads to localization in a manner similar to diagonal disorder [36–38]. However, near the band center ($E \rightarrow 0$), whether states remain localized or become extended remains a subject of debate [39, 40]. Except in this critical region, all states are exponentially localized for uncorrelated hopping amplitudes, regardless of the disorder strength. In contrast, introducing mosaic modulation ($\kappa \geq 2$) gives rise to distinct topological and localization features absent in conventional off-diagonal disordered systems, as we will demonstrate.

The degree of localization is quantitatively characterized by the IPR [41]. For the k -th eigenstate, represented by $(\psi_1^{(k)}, \psi_2^{(k)}, \dots, \psi_N^{(k)})^T$ with eigenvalue E_k , the IPR is defined as

$$\text{IPR}(E_k) = \frac{\sum_{n=1}^N |\psi_n^{(k)}|^4}{\left(\sum_{n=1}^N |\psi_n^{(k)}|^2\right)^2}. \quad (25)$$

The IPR ranges from zero for completely extended states to unity for states fully localized in the limit of infinite system size. In finite systems, extended states typically yield $\text{IPR} \sim O(1/L)$, while localized states exhibit $\text{IPR} \sim O(1)$.

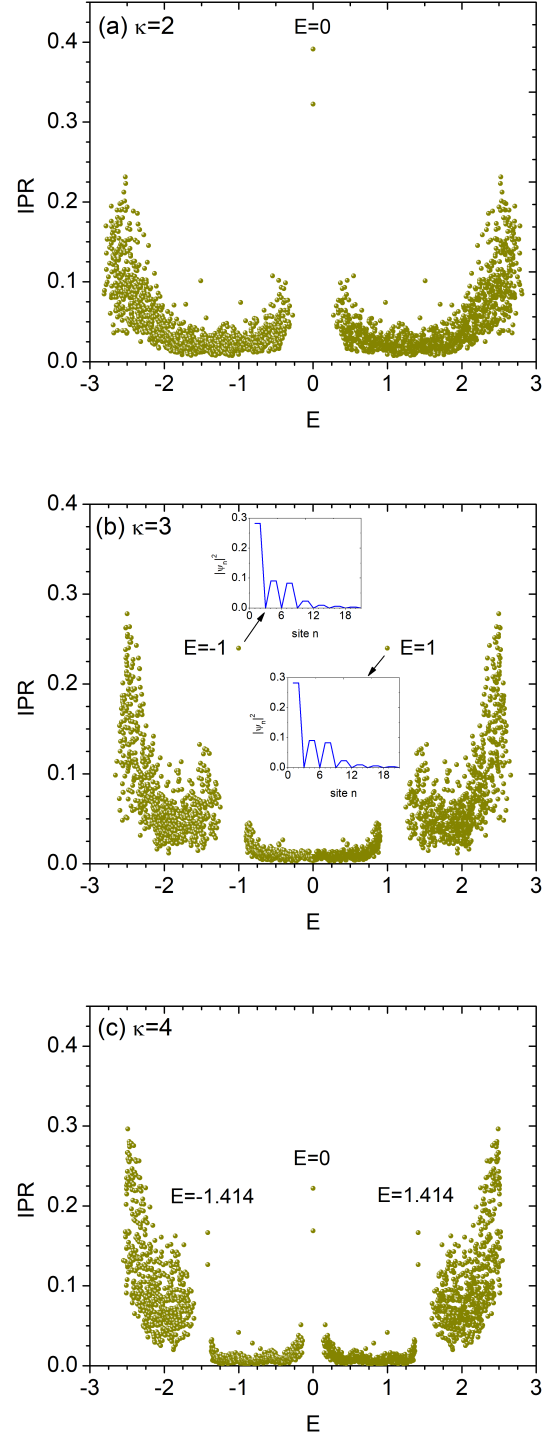


FIG. 7. Inverse participation ratio (IPR) as a function of energy E for a single random realization of a chain of length $L = 2000$ under open boundary conditions, with $\beta_0 = 1.5$, $m = 0$, and disorder strength $W = 1$. Results are shown for (a) $\kappa = 2$, (b) $\kappa = 3$ (Case 2 in Table I), and (c) $\kappa = 4$ (Case 1 in Table II). Edge states appear in pairs in (a) and (c), and individually in (b). The insets in (b) show that the node structure of the edge state remains robust against disorder.

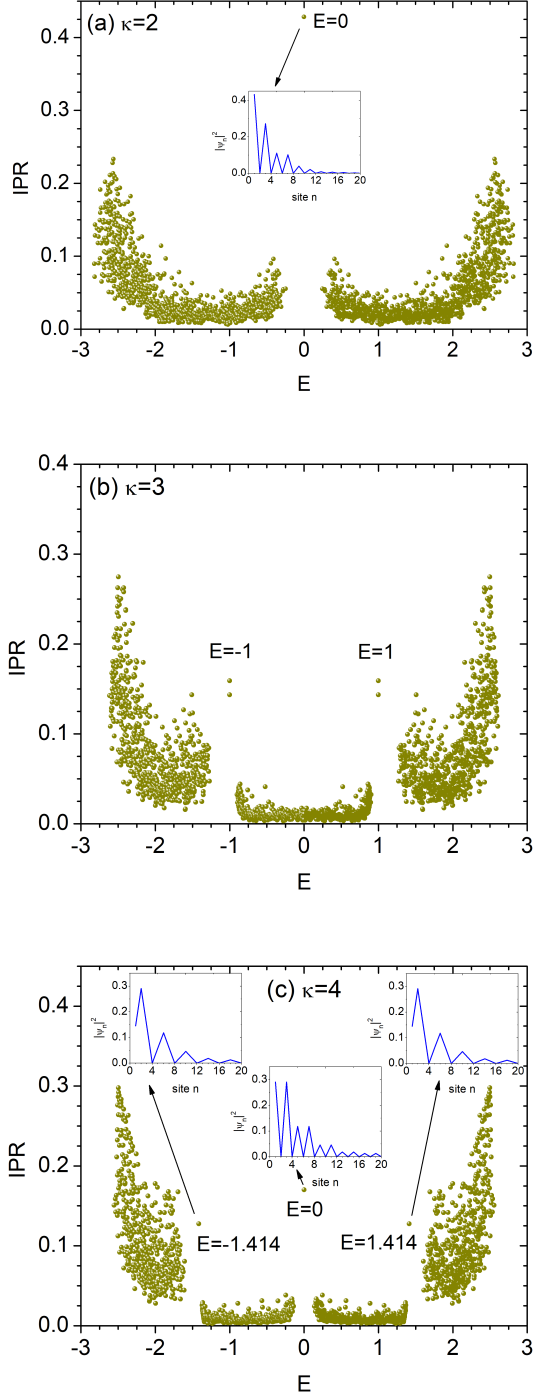


FIG. 8. IPR as a function of energy E for a single random realization of a chain of length $L = 2001$ under open boundary conditions, with $\beta_0 = 1.5$, $m = 0$, and disorder strength $W = 1$. Results are shown for (a) $\kappa = 2$, (b) $\kappa = 3$ (Case 1 in Table I), and (c) $\kappa = 4$ (Case 4 in Table II). Edge states appear in pairs in (b), and individually in (a) and (c). The insets in (a) and (c) show that the node structure of the topological edge state remains robust against disorder. In (c), however, edge states at $E = \pm\sqrt{1 + \beta^2}$ are absent due to the relatively strong disorder.

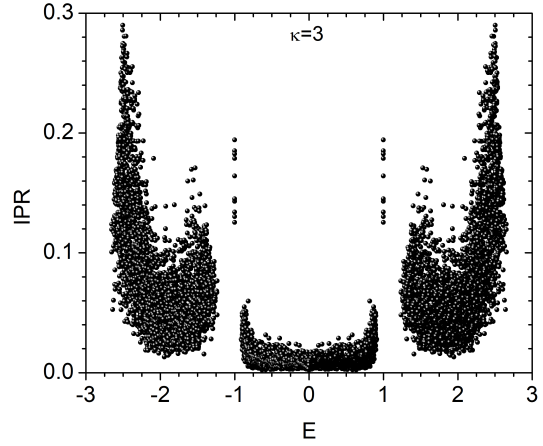


FIG. 9. IPR versus energy E for a chain of length $L = 2001$ under open boundary conditions, with $\kappa = 3$, $\beta_0 = 1.5$, $m = 0$, and disorder strength $W = 1$. Data from five independent random realizations are overlaid. In all cases, edge states consistently appear in pairs at $E = \pm 1$.

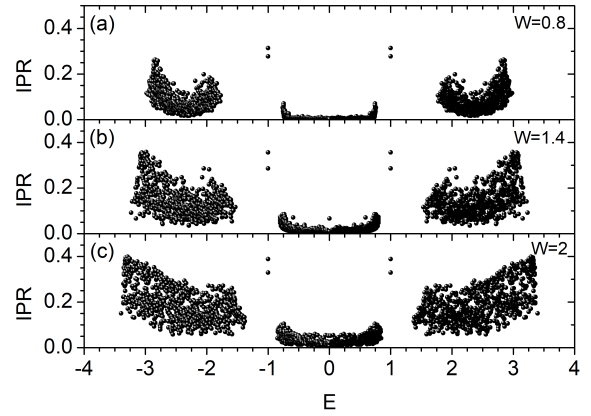


FIG. 10. IPR versus energy E for a single random realization of a chain of length $L = 2001$ under open boundary conditions, with $\kappa = 3$, $\beta_0 = 2$, $m = 0$, and disorder strengths $W = 0.8, 1.4$, and 2 . In all cases, edge states appear in pairs at $E = \pm 1$.

To compute the eigenvalues E and eigenstates $\psi = (\psi_1, \psi_2, \dots, \psi_N)^T$ in the presence of off-diagonal disorder, we numerically solve the eigenvalue problem $\hat{H}\psi = E\psi$, where \hat{H} is the disordered off-diagonal mosaic

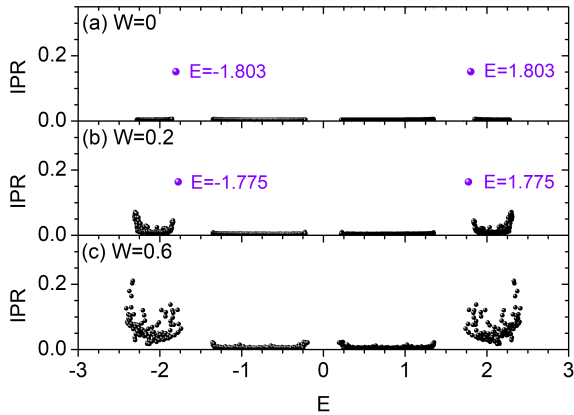


FIG. 11. IPR versus energy E for a single random realization of a chain of length $L = 400$ under open boundary conditions, with $\kappa = 3$, $\beta_0 = 2$, $m = 1$, and disorder strengths $W = 0, 0.2$, and 0.6 (Case 7 in Table II). In panels (a) and (b), edge states appear in pairs at $E \approx \pm\sqrt{1 + \beta^2}$, but they are absent in (c).

Hamiltonian:

$$\hat{H} = \begin{pmatrix} \epsilon & t_1 & 0 & \cdots & 0 & 0 & 0 \\ t_1 & \epsilon & t_2 & \cdots & 0 & 0 & 0 \\ 0 & t_2 & \epsilon & \cdots & 0 & 0 & 0 \\ \vdots & \vdots & \vdots & \ddots & \vdots & \vdots & \vdots \\ 0 & 0 & 0 & \cdots & \epsilon & t_{N-2} & 0 \\ 0 & 0 & 0 & \cdots & t_{N-2} & \epsilon & t_{N-1} \\ 0 & 0 & 0 & \cdots & 0 & t_{N-1} & \epsilon \end{pmatrix}. \quad (26)$$

Figures 7 and 8 show the IPR as a function of energy E for single random realizations in lattice chains of length $L = 2000$ and $L = 2001$, with $\kappa = 2, 3$, and 4 at $W = 1$. In all cases, the edge configuration has $m = 0$ and the first $(\kappa - 1)$ bonds on the left edge are long bonds. The examples for $\kappa = 3$ and 4 correspond to selected configurations from Tables I and II. The numerical results reveal that all eigenstates are localized, including those far from the band edges, where the IPR values remain comparatively small. Two types of localized states are observed: edge states and bulk states.

The localization properties exhibit several notable features. First, the IPR spectra are arranged into distinct clusters separated by band gaps, in contrast to conventional off-diagonal disordered systems ($\kappa = 1$), where such gaps are absent. As discussed earlier, the emergence of band gaps is a characteristic feature of the periodic off-diagonal mosaic model and persists under disorder. Second, within each band gap, isolated points appear either in pairs or singly, depending on κ and N . Analysis of the corresponding wave functions confirms that these isolated points represent topological edge states. These states preserve the same nodal structures as in the disorder-free case and remain robust against disorder.

Importantly, these states occur at energies satisfying the analytical expression Eq. (1), highlighting their topological protection within the disordered mosaic lattice. In contrast, localized bulk states are distributed arbitrarily throughout the system.

In related work on the diagonal disordered mosaic lattice, recent studies have identified discrete energy values at which eigenstates exhibit anomalous power-law localization [23, 24]. These states show distinctive nodal structures arising from the interplay of randomness and band structure. Similarly, we observe that all topological states in the disordered off-diagonal mosaic lattice display intrinsic node patterns. This is illustrated in the inset of Fig. 7(b) for $\kappa = 3$ and Fig. 8(a) and (c) for $\kappa = 2$ and 4 , where wave function zeros occur at all sites $j\kappa$ for any integer j .

To test the robustness of these topological states under different disorder realizations, Fig. 9 shows the IPR as a function of E for five independent random configurations in a chain of size $L = 2001$ with $\kappa = 3$. Each band gap contains ten isolated points corresponding to the ten edge states predicted for these configurations. The associated eigenvalues remain precisely at ± 1 , demonstrating their robustness against disorder.

Figure 10 presents results for a single random realization ($L = 2001$, $\kappa = 3$) at three different disorder strengths W . As in typical disordered systems, both edge and bulk localized states exhibit increasing IPR values with larger W , and the band gap width progressively decreases.

Finally, in Fig. 11, we examine the disorder dependence of the β -dependent edge states. For small W , these states persist but shift slightly in energy due to changes in the effective average β . However, at sufficiently large W , these β -dependent edge states are destroyed. We conclude that, unlike the topological edge states satisfying Eq. (1), the β -dependent edge states lack robustness against disorder.

V. CONCLUSION

We have systematically analyzed the emergence and robustness of topological edge states in 1D off-diagonal mosaic lattices with periodic and disordered hopping modulations. By extending the formalism of the SSH model to arbitrary mosaic periods $\kappa > 1$, we derived exact analytical expressions for the energy eigenvalues of edge states, $E = \epsilon + 2t \cos(\pi i/\kappa)$, and demonstrated their existence across a broad class of multi-band systems. Numerical simulations confirmed these predictions, revealing that the edge states exhibit characteristic nodal structures and are strongly influenced by the configurations of long and short bonds at the lattice boundaries.

We further explored the effects of off-diagonal disorder, showing that topological edge states retain their localization and energy eigenvalues even under significant hopping fluctuations, underscoring their robustness. In

contrast, additional β -dependent edge states, present for $\kappa \geq 4$, are highly sensitive to disorder and vanish as randomness increases.

These results provide a unified framework for understanding and engineering multi-gap topological phases in off-diagonal systems. They pave the way for realizing disorder-resilient edge states in synthetic quantum materials, photonic crystals, and other engineered lattices. Future work could explore their dynamical properties, interactions with external fields, and potential applications

in robust waveguiding and topological quantum information processing.

ACKNOWLEDGMENTS

This research was supported by the Basic Science Research Program through the National Research Foundation of Korea (<https://ror.org/013aysd81>) funded by the Ministry of Education (RS-2021-NR060141).

-
- [1] S.-Q. Shen, *Topological Insulators* (Springer, Berlin, 2012).
 - [2] B. A. Bernevig and T. L. Hughes, *Topological Insulators and Topological Superconductors* (Princeton University Press, Princeton, NJ, 2013).
 - [3] J. E. Moore, The birth of topological insulators, *Nature* **464**, 194 (2010).
 - [4] M. Z. Hasan and C. L. Kane, Colloquium: Topological insulators, *Rev. Mod. Phys.* **82**, 3045 (2010).
 - [5] X.-L. Qi and S.-C. Zhang, Topological insulators and superconductors, *Rev. Mod. Phys.* **83**, 1057 (2011).
 - [6] C. L. Kane and E. J. Mele, Quantum spin Hall effect in graphene, *Phys. Rev. Lett.* **95**, 226801 (2005).
 - [7] C. L. Kane and E. J. Mele, Z_2 topological order and the quantum spin Hall effect, *Phys. Rev. Lett.* **95**, 146802 (2005).
 - [8] L.-J. Lang, X. Cai, and S. Chen, Edge states and topological phases in one-dimensional optical superlattices, *Phys. Rev. Lett.* **108**, 220401 (2012).
 - [9] H. Guo and S. Chen, Kaleidoscope of symmetry-protected topological phases in one-dimensional periodically modulated lattices, *Phys. Rev. B* **91**, 041402(R) (2015).
 - [10] W. P. Su, J. R. Schrieffer, and A. J. Heeger, Solitons in polyacetylene, *Phys. Rev. Lett.* **42**, 1698 (1979).
 - [11] F. D. M. Haldane, Model for a quantum Hall effect without Landau levels: Condensed-matter realization of the “parity anomaly”, *Phys. Rev. Lett.* **61**, 2015 (1988).
 - [12] J. K. Asbóth, L. Oroszlány, and A. Pályi, *A Short Course on Topological Insulators: Band Structure and Edge States in One and Two Dimensions* (Springer, Berlin, 2016).
 - [13] J. Zak, Berry’s phase for energy bands in solids, *Phys. Rev. Lett.* **62**, 2747 (1989).
 - [14] V. M. Martinez Alvarez and M. D. Coutinho-Filho, Edge states in trimer lattices, *Phys. Rev. A* **99**, 013833 (2019).
 - [15] Y. Zhang, B. Ren, Y. Li, and F. Ye, Topological states in the super-SSH model, *Opt. Express* **29**, 42827 (2021).
 - [16] M. Eliashvili, D. Kereselidze, G. Tsitsishvili, and M. Tsitsishvili, Edge states of a periodic chain with four-band energy spectrum, *J. Phys. Soc. Jpn.* **86**, 074712 (2017).
 - [17] S. Bid and A. Chakrabarti, Topological properties of a class of Su-Schrieffer-Heeger variants, *Phys. Lett. A* **423**, 127816 (2022).
 - [18] Y. Wang, X. Xia, L. Zhang, H. Yao, S. Chen, J. You, Q. Zhou, and X.-J. Liu, One-dimensional quasiperiodic mosaic lattice with exact mobility edges, *Phys. Rev. Lett.* **125**, 196604 (2020).
 - [19] Q.-B. Zeng, R. Lü, and L. You, Topological superconductors in one-dimensional mosaic lattices, *EPL* **135**, 17003 (2021).
 - [20] Q.-B. Zeng and R. Lü, Topological phases and Anderson localization in off-diagonal mosaic lattices, *Phys. Rev. B* **104**, 064203 (2021).
 - [21] L.-Y. Gong, H. Lu, and W.-W. Cheng, Exact mobility edges in 1D mosaic lattices inlaid with slowly varying potentials, *Adv. Theory Simul.* **4**, 2100135 (2021).
 - [22] D. Dwiputra and F. P. Zen, Single-particle mobility edge without disorder, *Phys. Rev. B* **105**, L081110 (2022).
 - [23] B. P. Nguyen, D. K. Phung, and K. Kim, Quasiresonant diffusion of wave packets in one-dimensional disordered mosaic lattices, *Phys. Rev. B* **106**, 134204 (2022).
 - [24] B. P. Nguyen and K. Kim, Transport and localization properties of excitations in one-dimensional lattices with diagonal disordered mosaic modulations, *J. Phys. A: Math. Theor.* **56**, 475701 (2023).
 - [25] M. Atala, M. Aidelsburger, J. T. Barreiro, D. Abanin, T. Kitagawa, E. Demler, and I. Bloch, Direct measurement of the Zak phase in topological Bloch bands, *Nat. Phys.* **9**, 795 (2013).
 - [26] Y. He, K. Wright, S. Kouachi, and C.-C. Chien, Topology, edge states, and zero-energy states of ultracold atoms in one-dimensional optical superlattices with alternating on-site potentials or hopping coefficients, *Phys. Rev. A* **97**, 023618 (2018).
 - [27] Y. E. Kraus, Y. Lahini, Z. Ringel, M. Verbin, and O. Zilberberg, Topological states and adiabatic pumping in quasicrystals, *Phys. Rev. Lett.* **109**, 106402 (2012).
 - [28] M. Verbin, O. Zilberberg, Y. E. Kraus, Y. Lahini, and Y. Silberberg, Observation of topological phase transitions in photonic quasicrystals, *Phys. Rev. Lett.* **110**, 076403 (2013).
 - [29] M. Verbin, O. Zilberberg, Y. Lahini, Y. E. Kraus, and Y. Silberberg, Topological pumping over a photonic Fibonacci quasicrystal, *Phys. Rev. B* **91**, 064201 (2015).
 - [30] W. Zhu, S. Hou, Y. Long, H. Chen, and J. Ren, Simulating quantum spin Hall effect in the topological Lieb lattice of a linear circuit network, *Phys. Rev. B* **97**, 075310 (2018).
 - [31] J. Ningyuan, C. Owens, A. Sommer, D. Schuster, and J. Simon, Time- and site-resolved dynamics in a topological circuit, *Phys. Rev. X* **5**, 021031 (2015).
 - [32] M. Pan, H. Zhao, P. Miao, S. Longhi, and L. Feng, Photonic zero mode in a non-Hermitian photonic lattice, *Nat. Commun.* **9**, 1308 (2018).
 - [33] S. Xia, D. Kaltsas, D. Song, I. Komis, J. Xu, A. Szameit,

- H. Buljan, K. G. Makris, and Z. Chen, Nonlinear tuning of PT symmetry and non-Hermitian topological states, *Science* **372**, 72 (2021).
- [34] P. St-Jean, V. Goblot, E. Galopin, A. Lemaître, T. Ozawa, L. Le Gratiet, I. Sagnes, J. Bloch, and A. Amo, Lasing in topological edge states of a one-dimensional lattice, *Nat. Photonics* **11**, 651 (2017).
- [35] B. Beckermann, J. Gilewicz, and E. Leopold, Recurrence relations with periodic coefficients and Chebyshev polynomials, *Appl. Math.* **23**, 319 (1995).
- [36] P. W. Anderson, Absence of diffusion in certain random lattices, *Phys. Rev.* **109**, 1492 (1958).
- [37] P. A. Lee and T.V. Ramakrishnan, Disordered electronic systems, *Rev. Mod. Phys.* **57**, 287 (1985).
- [38] F. Evers and A. D. Mirlin, Anderson transitions, *Rev. Mod. Phys.* **80**, 1355 (2008).
- [39] H. Cheraghchi, S. M. Fazeli, and K. Esfarjani, Localization-delocalization transition in a one-dimensional system with long-range correlated off-diagonal disorder, *Phys. Rev. B* **72**, 174207 (2005).
- [40] F. M. Izrailev, A. A. Krokhnin, and N. M. Makarov, Anomalous localization in low-dimensional systems with correlated disorder, *Phys. Rep.* **512**, 125 (2012).
- [41] F. Wegner, Inverse participation ratio in $2+\epsilon$ dimensions, *Z. Phys. B* **36**, 209 (1980).